



# Rotation invariant texture classification using LBP variance (LBPV) with global matching

Zhenhua Guo, Lei Zhang, David Zhang \*

Biometrics Research Centre, Department of Computing, The Hong Kong Polytechnic University, Hung Hom, Kowloon, Hong Kong, China

## ARTICLE INFO

### Article history:

Received 24 April 2009  
Received in revised form  
2 July 2009  
Accepted 19 August 2009

### Keywords:

Texture classification  
Local binary pattern  
Rotation invariant  
Global matching

## ABSTRACT

Local or global rotation invariant feature extraction has been widely used in texture classification. Local invariant features, e.g. local binary pattern (LBP), have the drawback of losing global spatial information, while global features preserve little local texture information. This paper proposes an alternative hybrid scheme, globally rotation invariant matching with locally variant LBP texture features. Using LBP distribution, we first estimate the principal orientations of the texture image and then use them to align LBP histograms. The aligned histograms are then in turn used to measure the dissimilarity between images. A new texture descriptor, LBP variance (LBPV), is proposed to characterize the local contrast information into the one-dimensional LBP histogram. LBPV does not need any quantization and it is totally training-free. To further speed up the proposed matching scheme, we propose a method to reduce feature dimensions using distance measurement. The experimental results on representative databases show that the proposed LBPV operator and global matching scheme can achieve significant improvement, sometimes more than 10% in terms of classification accuracy, over traditional locally rotation invariant LBP method.

© 2009 Elsevier Ltd. All rights reserved.

## 1. Introduction

Texture analysis is an active research topic in the fields of computer vision and pattern recognition. It involves four basic problems: classifying images based on texture content; segmenting an image into regions of homogeneous texture; synthesizing textures for graphics applications; and establishing shape information from texture cues [1]. Among them, texture classification has been widely studied because it has a wide range of applications, such as fabrics inspection [2], remote sensing [3] and medical image analysis [4].

Early methods for texture classification focus on the statistical analysis of texture images. The representative methods include the co-occurrence matrix method [5] and filtering based approaches [6], such as Gabor filtering [7,8], wavelet transform [9,10] and wavelet frames [11]. In general their classification results are good as long as the training and test samples have identical or similar orientations. However, the rotations of real-world textures will vary arbitrarily, severely affecting the performance of the statistical methods and suggesting the need for rotation invariant methods of texture classification.

Kashyap and Khotanzad were among the first researchers to study rotation-invariant texture classification using a circular

autoregressive model [12]. Later models include the multiresolution autoregressive model [13], hidden Markov model [14,15], Gaussian Markov random field [21], and the autocorrelation model [20]. Many Gabor and wavelet based algorithms were also proposed for rotation invariant texture classification [16–19,22,25,26]. Ojala et al. [24] proposed using a local binary pattern (LBP) histogram for rotation invariant texture classification. Recently, Varma and Zisserman [23] presented a statistical algorithm, MR8, where a rotation invariant texture library is first built from a training set and then an unknown texture image is classified according to its texture distribution. The LBP and MR8 methods are both state-of-the-art algorithms and yield good classification results on large and complex databases [23,34]. Scale and affine invariance is another issue to be addressed in texture classification, and some pioneer works have been recently proposed by using affine adaption [36], fractal analysis [37] and combination of filters [38].

Many rotation invariant texture classification methods [12,13,23,24], such as LBP, extract rotation invariant texture features from a local region. However, such features may fail to classify the images. Fig. 1 shows an example. Fig. 1(a) and (b) are the LBP codes of two texture images, each of which is composed of two LBP micro-patterns. Obviously, each image exhibits different texture information, yet if the locally rotation invariant LBP micro-pattern in Fig. 1(c) is used to represent and classify the textures, the two images will be misclassified as of the same class. This is because we lose global image information when only the locally

\* Corresponding author.

E-mail address: [csdzhang@comp.polyu.edu.hk](mailto:csdzhang@comp.polyu.edu.hk) (D. Zhang).

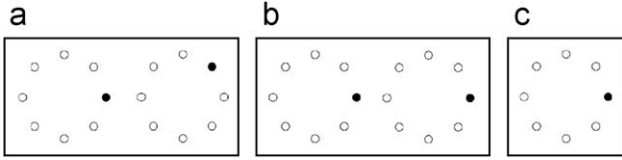


**Fig. 1.** (a, b) The LBP codes of two texture images, each of which is composed of two LBP micro-patterns. By using the LBP rotation invariant LBP micro-pattern in (c), the two different images will be misclassified as the same class.

rotation invariant features are used. Jafari-Khouzani and Soltanian-Zadeh [22] proposed a method to solve this problem. First, the Radon transform was used to estimate the principal orientation of the texture image and then the wavelet energy features were computed along the principal orientation. Unfortunately, using the Radon transform to align the image makes the computational cost of this method high.

A further difficulty associated with image texture classification is the robust and accurate representation of texture information. Generally, texture can be characterized by a spatial structure (e.g. a pattern such as LBP) and the contrast (e.g. VAR, the variance of local image texture) [24]. Spatial structures vary with rotation while contrast does not. Ojala et al. [24] proposed using the joint histogram of the two complementary features, namely LBP/VAR, for rotation invariant texture classification. The drawback of this approach is that the value of VAR is continuous so that a quantization step is needed to calculate the histogram. However, a good quantization depends upon a large number of and comprehensive training samples.

In this paper, we propose an efficient global matching scheme that uses LBP for feature extraction. Our approach does not extract locally rotation invariant LBP as in [24], but instead first builds a rotation variant LBP histogram and then applies a global matching procedure. This global matching can be implemented using an exhaustive search scheme such as [27,28] to find the minimal distance in all candidate orientations yet is nonetheless computationally extensive. Fortunately, the extracted LBP features can be used to estimate the principal orientations and hence we can compute the matching distances along the principal orientations only.

Our proposed approach also applies a joint histogram as in [24] but addresses the quantization problem by proposing a new operator called the Local Binary Pattern Variance (LBPV). Instead of computing the joint histogram of LBP and VAR globally, the LBPV computes the VAR from a local region and accumulates it into the LBP bin. This can be regarded as the integral projection [30] along the VAR coordinate. Associated with the proposed global matching scheme, the LBPV operator could reduce greatly the requirement for and dependency on a large number of training samples.

The rest of the paper is organized as follows. Section 2 briefly reviews the LBP and VAR, and then presents the proposed LBPV operator and the dissimilarity metric. Section 3 presents the proposed global matching scheme. Section 4 reports the experimental results on two comprehensive public texture databases. Section 5 gives the conclusion and future work.

## 2. Feature descriptor and dissimilarity metric

In this section, the LBP and VAR feature extractors are first reviewed. To address the limitation of VAR, the LBPV is then proposed. Finally, the matching dissimilarity metric in this work is presented.

### 2.1. LBP

LBP [24] is a gray-scale texture operator which characterizes the spatial structure of the local image texture. Given a central

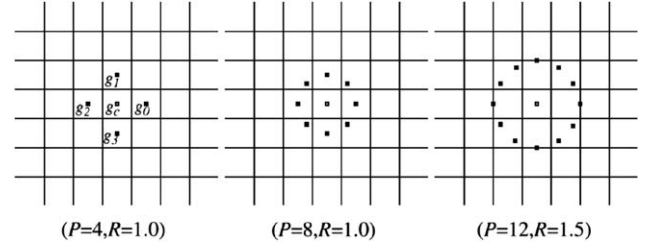


**Fig. 2.** Circular symmetric neighbor sets for different  $(P, R)$ .

pixel in the image, a pattern number is computed by comparing its value with those of its neighborhoods:

$$LBP_{P,R} = \sum_{p=0}^{P-1} s(g_p - g_c) 2^p \quad (1)$$

$$s(x) = \begin{cases} 1, & x \geq 0 \\ 0, & x < 0 \end{cases} \quad (2)$$

where  $g_c$  is the gray value of the central pixel,  $g_p$  is the value of its neighbors,  $P$  is the number of neighbors and  $R$  is the radius of the neighborhood. Suppose the coordinates of  $g_c$  are  $(0, 0)$ , then the coordinates of  $g_p$  are given by  $(-R \sin(2\pi p/P), R \cos(2\pi p/P))$ . Fig. 2 shows examples of circularly symmetric neighbor sets for different configurations of  $(P, R)$ . The gray values of neighbors that are not in the center of grids can be estimated by interpolation.

Suppose the texture image is  $N \times M$ . After identifying the LBP pattern of each pixel  $(i, j)$ , the whole texture image is represented by building a histogram:

$$H(k) = \sum_{i=1}^N \sum_{j=1}^M f(LBP_{P,R}(i, j), k), k \in [0, K] \quad (3)$$

$$f(x, y) = \begin{cases} 1, & x = y \\ 0, & \text{otherwise} \end{cases} \quad (4)$$

where  $K$  is the maximal LBP pattern value. The  $U$  value of an LBP pattern is defined as the number of spatial transitions (bitwise 0/1 changes) in that pattern

$$U(LBP_{P,R}) = |s(g_{P-1} - g_c) - s(g_0 - g_c)| + \sum_{p=1}^{P-1} |s(g_p - g_c) - s(g_{p-1} - g_c)| \quad (5)$$

For example, LBP pattern 00000000 has a  $U$  value of 0 and 01000000 of 2. The uniform LBP pattern refers to the uniform appearance pattern which has limited transition or discontinuities ( $U \leq 2$ ) in the circular binary presentation [24]. It was verified that only “uniform” patterns are fundamental patterns of local image texture.

Fig. 3 shows all uniform patterns for  $P=8$ . All the non-uniform patterns ( $U > 2$ ) are grouped under a “miscellaneous” label. In practice, the mapping from  $LBP_{P,R}$  to  $LBP_{P,R}^{u2}$  (superscript “u2” means that the uniform patterns have  $U$  values of at most 2), which has  $P^*(P-1)+3$  distinct output values, is implemented with a lookup table of  $2^P$  elements.

As shown in each of the first seven rows of Fig. 3, any one of the eight patterns in the same row is a rotated version of the others. So a locally rotation invariant pattern could be defined as

$$LBP_{P,R}^{riu2} = \begin{cases} \sum_{p=0}^{P-1} s(g_p - g_c) & \text{if } U(LBP_{P,R}) \leq 2 \\ P+1 & \text{otherwise} \end{cases} \quad (6)$$

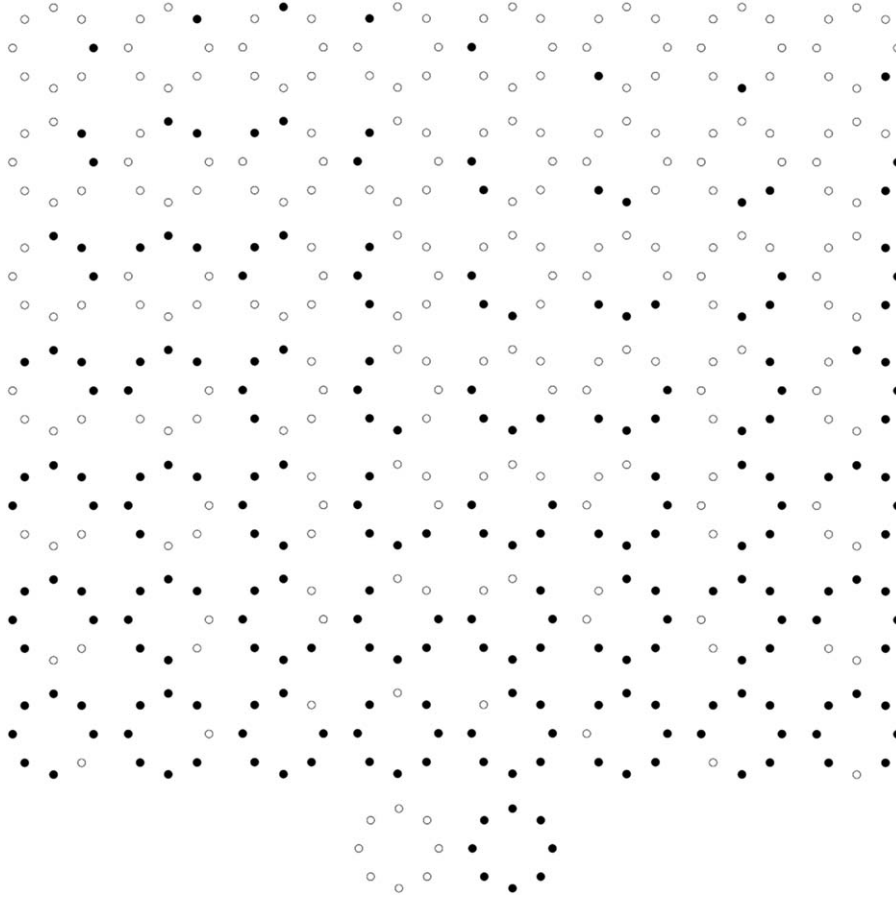


Fig. 3. Uniform LBP patterns when  $P=8$ . The black and white dots represent the bit values of 1 and 0 in the 8-bit output of the LBP operator.

Similar to  $LBP_{P,R}^{u2}$ , the mapping from  $LBP_{P,R}$  to  $LBP_{P,R}^{riu2}$ , which has  $P+2$  distinct output value, can be implemented with a lookup table.

### 2.2. Rotation invariant variance measures (VAR)

A rotation invariant measure of the local variance can be defined as [24]

$$VAR_{P,R} = \frac{1}{P} \sum_{p=0}^{P-1} (g_p - u)^2 \quad (7)$$

where  $u = 1/P \sum_{p=0}^{P-1} g_p$ . Since  $LBP_{P,R}$  and  $VAR_{P,R}$  are complementary, their joint distribution  $LBP_{P,R}/VAR_{P,R}$  can better characterize the image local texture than using  $LBP_{P,R}$  alone. Although Ojala et al. [24] proposed to use only the joint distribution  $LBP_{P,R}^{riu2}/VAR_{P,R}$  of  $LBP_{P,R}^{riu2}$  and  $VAR_{P,R}$ , other types of patterns, such as  $LBP_{P,R}^{u2}$ , can also be used jointly with  $VAR_{P,R}$ . However,  $LBP_{P,R}^{u2}$  is not rotation invariant and it has higher dimensions. In practice, the same  $(P, R)$  values are used for  $LBP_{P,R}^{riu2}$  and  $VAR_{P,R}$ .

### 2.3. LBP variance (LBPV)

$LBP_{P,R}/VAR_{P,R}$  is powerful because it exploits the complementary information of local spatial pattern and local contrast [24]. However,  $VAR_{P,R}$  has continuous values and it has to be quantized. This can be done by first calculating feature distributions from all training images to get a total distribution and then, to guarantee the highest quantization resolution, some threshold values are computed to partition the total distribution into  $N$  bins with an equal number of entries. These threshold values are used to quantize the VAR of the test images.

There are three particular limitations to this quantization procedure. First, it requires a training stage to determine the threshold value for each bin. Second, because different classes of textures may have very different contrasts, the quantization is dependent on the training samples. Last, there is an important parameter, i.e. the number of bins, to be preset. Too few bins will fail to provide enough discriminative information while too many bins may lead to sparse and unstable histograms and make the feature size too large. Although there are some rules to guide selection [24], it is hard to obtain an optimal number of bins in terms of accuracy and feature size.

The LPBV descriptor proposed in this section offers a solution to the above problems of  $LBP_{P,R}/VAR_{P,R}$  descriptor. The LBPV is a simplified but efficient joint LBP and contrast distribution method. As can be seen in Eq. (3), calculation of the LBP histogram  $H$  does not involve the information of variance  $VAR_{P,R}$ . That is to say, no matter what the LBP variance of the local region, histogram calculation assigns the same weight 1 to each LBP pattern. Actually, the variance is related to the texture feature. Usually the high frequency texture regions will have higher variances and they contribute more to the discrimination of texture images [8]. Therefore, the variance  $VAR_{P,R}$  can be used as an adaptive weight to adjust the contribution of the LBP code in histogram calculation. The LBPV histogram is computed as

$$LBPV_{P,R}(k) = \sum_{i=1}^N \sum_{j=1}^M w(LBP_{P,R}(i,j), k), k \in [0, K] \quad (8)$$

$$w(LBP_{P,R}(i,j), k) = \begin{cases} VAR_{P,R}(i,j), & LBP_{P,R}(i,j) = k \\ 0 & \text{otherwise} \end{cases} \quad (9)$$

If we view LBP and VAR as the two orthogonal axes in a coordinate system, the LBPV could be regarded as an integral projection [30] along the VAR axis. This would be a simplified representation of the 2D LBP/VAR distribution. Because  $LBPV_{P,R}^{u2}$  ( $LBPV_{P,R}^{riu2}$ ) is a simplified descriptor of  $LBP_{P,R}^{u2}/VAR_{P,R}$  ( $LBP_{P,R}^{riu2}/VAR_{P,R}$ ), its feature size is much smaller than that of  $LBP_{P,R}^{u2}/VAR_{P,R}$  ( $LBP_{P,R}^{riu2}/VAR_{P,R}$ ) and is the same as that of  $LBP_{P,R}^{u2}$  ( $LBP_{P,R}^{riu2}$ ). Furthermore, it can be seen that the proposed LBPV is training free and it does not need quantization.

2.4. Dissimilarity metric

The dissimilarity of sample and model histograms is a test of goodness-of-fit, which can be measured with a non-parametric statistic test. There are many metrics for evaluating the fit between two histograms, such as histogram intersection, log-likelihood ratio, and chi-square statistic [24]. In this study, a test sample  $S$  was assigned to the class of model  $M$  that minimizes the chi-square distance:

$$D(S, M) = \sum_{n=1}^N \frac{(S_n - M_n)^2}{S_n + M_n} \tag{10}$$

where  $N$  is the number of bins and  $S_n$  and  $M_n$  are, respectively, the values of the sample and model images at the  $n$ th bin. Here, we use the nearest neighborhood classifier with chi-square distance because it is equivalent to the optimal Bayesian classification [31].

3. Rotation invariant global matching

In this section, we describe our global matching scheme, namely rotation invariant global matching. The reasoning behind our proposed scheme can be seen by again considering Fig. 3. It shows eight rows of patterns in which each of the first seven rows shows a rotated version of the same pattern. Traditionally, LBP histogram calculation achieves rotation invariance by clustering each row into one bin. However, as was illustrated in Fig. 1, such an operation loses the global information, and hence two different texture images may have the same number of locally rotation invariant patterns. In Fig. 3, each column in the first seven rows is a 45° or -45° rotation of its adjacent column. Fig. 4 shows another example. Suppose an image contains 256 (i.e.  $P=8$ ) possible LBP patterns and the frequency with which each pattern occurs in the image is represented by the number in the pattern, as shown in Fig. 4(a). If the image is rotated 90° clockwise, then a new LBP histogram will be created, and Fig. 4(a) becomes (b).

This observation suggests the feasibility of designing a rotation invariant matching scheme using rotation variant LBP patterns. This could be done by exhaustively searching for the minimal distance from all candidate orientations [27,28] but that would be computationally prohibitive. Rather, our proposed global matching scheme first uses the extracted LBP features to estimate the principal orientations, and then aligns the features to the principal orientations to compute the matching distance. Further feature dimension reduction can be achieved by reducing less important patterns.

3.1. Matching by exhaustive search

The exhaustive matching search method is simple and intuitive. Taking Fig. 4 as an example,<sup>1</sup> the LBP histogram can be divided into two sets: the first seven rows being rotation variant

and the last row being rotation invariant. For a given sample, we shift one column of the first seven rows and compute the dissimilarity with the models. This procedure is iteratively run eight times to find the minimal dissimilarity as the final distance. To present the method explicitly, the LBP histogram is reorganized and represented by two matrixes,  $H^{rv}$  (rotation variant histogram) and  $H^{ri}$  (rotation invariant histogram), as shown in Fig. 5. Then for any two texture images, the matching distance could be calculated as

$$D_{ES}(H_S, H_M) = D_{\min}(H_S^{ri}, H_M^{ri}) + D_{rv}(H_S^{rv}, H_M^{rv})$$

$$\begin{cases} D_{ri}(H_S^{ri}, H_M^{ri}) = D(H_S^{ri}, H_M^{ri}) \\ D_{\min}(H_S^{rv}, H_M^{rv}) = \min(D(H_S^{rv}, \overline{H_M^{rv}(j)})), j = 0, 1, \dots, 7 \\ \overline{H_M^{rv}(j)} = [h_{\text{mod}(0-j,8)}^M, h_{\text{mod}(1-j,8)}^M, \dots, h_{\text{mod}(7-j,8)}^M] \end{cases} \tag{11}$$

where  $\text{mod}(x, y)$  is the modulus  $x$  of  $y$ ,  $D(X, Y)$  is the chi-square distance defined in Eq. (10),  $H_S$  and  $H_M$  are the LBP histograms of a sample and model image, and  $\overline{H^{rv}(j)}$  is the new matrix which is obtained by shifting  $j$  columns of the original matrix  $H^{rv}$ . From Eq. (11) we see that the distance between two given histograms is composed by two parts: one ( $D_{ri}(H_S^{ri}, H_M^{ri})$ ) is derived from rotation invariant part ( $H_{ri}$ ), and the other one ( $D_{\min}(H_S^{rv}, H_M^{rv})$ ) is obtained by searching the minimal distance within rotation variant part ( $H^{rv}$ ).

Although the exhaustive matching method is simple and intuitive, it is computationally expensive because the feature dimension can be very high. For example, when  $P=24$ , using (11), we need to compute the chi-square distance between two feature sets of  $(24 \times 23 + 3) = 555$  dimensions along 24 orientations (equivalent to compute chi-square distance between two features of  $(24 \times 23 \times 24 + 3) = 13251$  dimensions) for all the models. Such a high complexity may prohibit the real time application of texture recognition. Therefore, a fast matching scheme must be developed to reduce the computational cost.

3.2. Global matching along principal orientations

It is also intuitive that if a principal orientation could be estimated for the test image, then the distance can be computed with the features aligned by that orientation. In this way the matching complexity can be reduced significantly. Similar idea has been exploited by Jafari-Khouzani and Soltanian-Zadeh [22]. However, this algorithm uses Radon transform to estimate the orientation of the texture image and requires much computational cost. In this section, we proposed to use LBP features to estimate the principal orientations directly.

In the first seven rows of Fig. 5, we can see that the accumulated histogram along one column corresponds to how many patterns are in one orientation. Because most of these patterns are edges of varying positive and negative curvatures [24], the orientation along which there is a peak of the histogram could be defined as a principal orientation of the texture image. Fig. 6 shows an example. Fig. 6(a) and (b) are the same texture captured under different orientations. The accumulated histograms along different orientation are plotted in Fig. 6(c) and (d). We see that 90° will be the principal orientation of Fig. 6(a) and 0° the principal orientation of Fig. 6(b) (the two images are not the identical images, so their LBP histograms are not shifted equally).

Owing to the complexity of structure of some textures, some images may have multiple peaks, i.e. multiple principal orientations. If only one principal orientation is preserved we may sometimes fail to get a good alignment of the texture. For example, for the same texture in Fig. 7, if only selecting one principal orientation, the principal orientation of Fig. 7(a) will be 270°, while that of Fig. 7(b) is 315°. The two images will not be

<sup>1</sup> For simplicity, only  $P=8$  is presented in this section to explain the matching scheme. The method is applied to  $P=16$  or 24 in the same way.

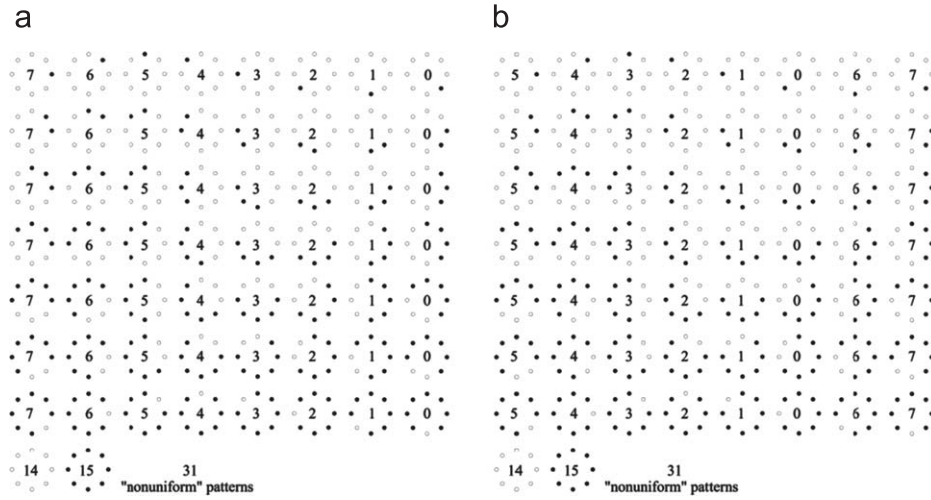


**Fig. 4.** The LBP histogram on the left is rotated 90° clockwise to become the histogram on the right. The number in each pattern represents how often that pattern occurs in the image. (a) LBP histogram of the original image and (b) LBP histogram of rotated image (90° clockwise).

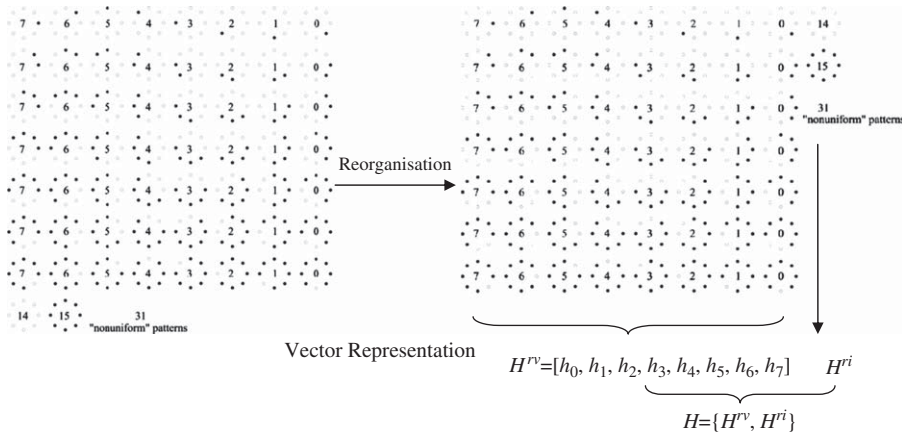


**Fig. 5.** The vector representation of histogram for  $P=8$ .

aligned correctly if only one orientation is kept. While, the second principal orientation of Fig. 7(a) and (b) are 315° and 270°, respectively (because of the symmetry, the difference between the first and second principal orientation should not be 180°), which are accordance with the first principal orientation of Figs 7(b) and (a). Therefore, if two principal orientations are used for matching, better classification results can be expected. Similar to Eq. (11), the dissimilarity between two images is computed as follows:

$$D_{PD2}(H_S, H_M) = D_{\min}(H_S^{rv}, H_M^{rv}) + D_{ri}(H_S^{ri}, H_M^{ri}) \quad (12)$$

with

$$D_{\min}(H_S^{rv}, H_M^{rv}) = \min\{D(H_S^{rv}, \overline{H_M^{rv}(j_{PD1}^M)}), D(H_S^{rv}, \overline{H_M^{rv}(j_{PD2}^M)})\}, \quad (13)$$

$$D(H_S^{rv}(j_{PD1}^S), H_M^{rv}), D(H_S^{rv}(j_{PD2}^S), H_M^{rv})\}$$

where  $j_{PD1}^S$  ( $j_{PD2}^S$ ) and  $j_{PD1}^M$  ( $j_{PD2}^M$ ), respectively, represent the first and second principal orientations of  $S(M)$ .

### 3.3. Feature dimension reduction

The use of principal orientations can significantly speed up feature matching but it does not reduce the dimensionality of features. For example, using  $P=24$  and Eq. (12) is equivalent to compute the chi-square distance between two feature vectors of  $(24 \times 23 \times 4 + 3) = 2211$  dimensions. Clearly, this is not acceptable

for high speed and real time applications. In this paper, we propose a simple and efficient feature reduction method that makes use of the feature distribution and dissimilarity metric.

From Eqs. (12) and (13), we see that the high dimensionality of features is caused by keeping all of rotation variant texture patterns. As shown in the first seven rows of Fig. 4, there are  $8 \times 7 = 56$  patterns and each row corresponds to a rotation invariant pattern. If a row is clustered into its rotation invariant pattern, using the same matching scheme above, the dimension could be reduced. In some sense, this can be viewed as a hybrid matching scheme, which works on rotation invariant features and rotation variant features with a rotation invariant matching. In the extreme case, all rows are clustered into their corresponding rotation invariant patterns, this is equivalent to the traditional  $LBP_{P,R}^{riu2}$ .

The chi-square distance in Eq. (10) could be rewritten as follows, which could be regarded as a weighted  $L^2$ -norm:

$$D(S, M) = \sum_{n=1}^N \frac{(S_n - M_n)^2}{S_n + M_n} = \sum_{n=1}^N \left( \frac{1}{S_n + M_n} \right) * (S_n - M_n)^2 \quad (14)$$

where  $1/S_n + M_n$  can be viewed as the weight and is inversely proportional to the sum of frequencies of two histograms at one bin. Thus, clustering more frequent patterns into rotation invariant patterns will have little influence on accuracy because  $1/S_n + M_n$  will be very small.

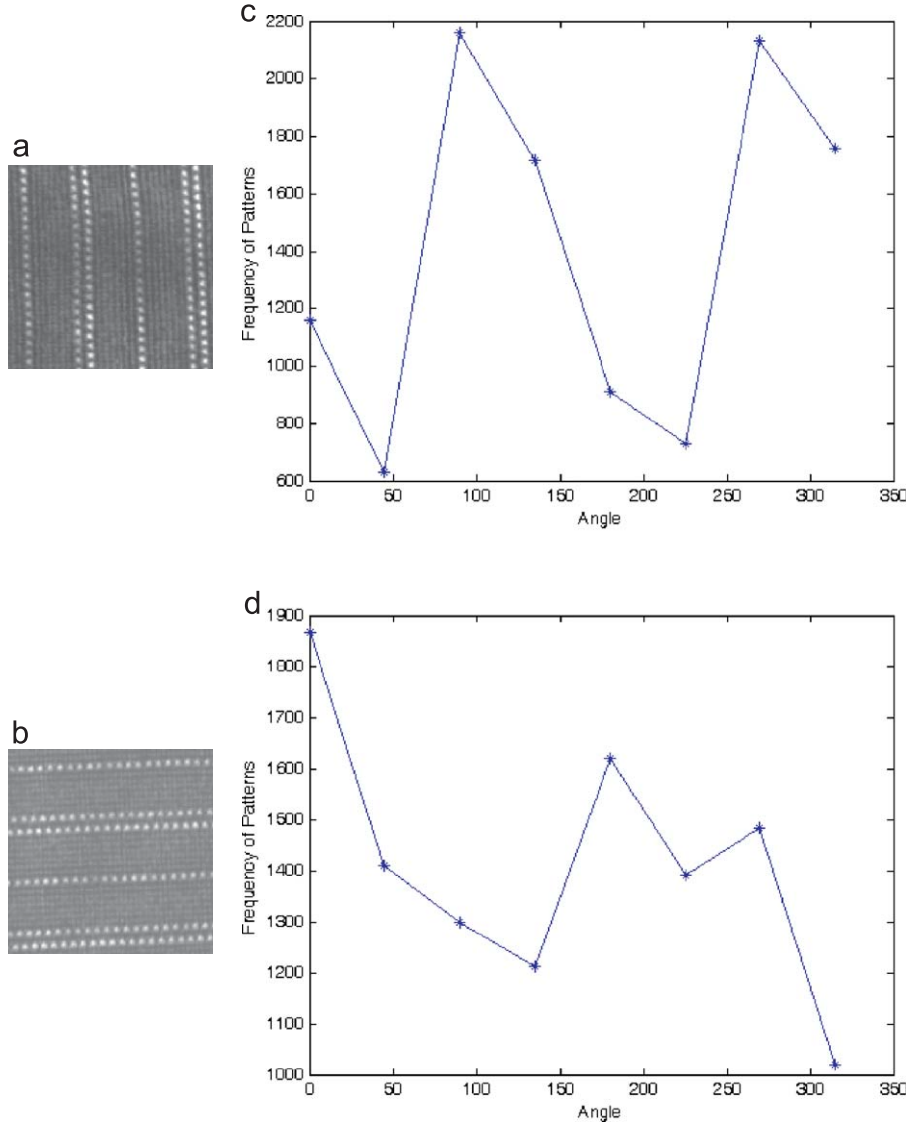


Fig. 6. One principal orientation texture sample: (a) canvas006 0° [32]; (b) canvas006 90°; (c)  $LBP_{8,1}^{riu2}$  pattern frequency versus angle for image (a); and (d)  $LBP_{8,1}^{riu2}$  pattern frequency versus angle for image (b).

Taking Fig. 4 as an example, a new histogram  $H' = [H'_1, H'_2, \dots, H'_7]$  for the whole training set is computed by accumulating each row into one bin for every image:

$$H'_j = \sum_{i=1}^N H^i_j, j = 1, 2, \dots, 7 \quad (15)$$

where  $H^i_j$  is the value of the  $j$ th bin in the  $i$ th image and  $N$  is the number of training images. The new histogram  $H'$  is sorted in descending order,  $H'' = [H''_1, H''_2, \dots, H''_7], H''_i \geq H''_j$  if  $i \leq j$ . As each bin in  $H''$  corresponds to one row of Fig. 4, the row corresponding to the largest value bin will be clustered into one rotation invariant pattern. Fig. 8 shows an example of before and after one step feature reduction. In Fig. 8, the third row in Fig. 8(a) is clustered into one pattern, marked in the rectangle of Fig. 8(b). This reduces the number of histogram bins from 59 to 52. This procedure is repeated to remove the largest bin in the remaining of  $H''$  until desired dimension is reached. The test set will reduce their LBP histogram dimension according to the training procedure.

The dissimilarity metric is defined as

$$D_{PD2}^{RN}(H_S^{RN}, H_M^{RN}) = D_{\min}(H_S^{RNrv}, H_M^{RNrv}) + D(H_S^{RNri}, H_M^{RNri}) \quad (16)$$

with

$$D_{\min}(H_S^{RNrv}, H_M^{RNrv}) = \min(D(H_S^{RNrv}, \overline{H_M^{RNrv}(j_{PD1}^M)}), D(H_S^{RNrv}, \overline{H_M^{RNrv}(j_{PD2}^M)}), D(\overline{H_S^{RNrv}(j_{PD1}^S)}, H_M^{RNrv}), D(\overline{H_S^{RNrv}(j_{PD2}^S)}, H_M^{RNrv})) \quad (17)$$

where  $RN$  is the number of remaining rows of rotation variant patterns.  $H^{RN}$  is the new histogram after feature reduction. For example,  $RN=7$  in Fig. 8(a) and  $RN=6$  in Fig. 8(b). Similar to what is shown in Fig. 5,  $H^{RNrv}$  and  $H^{RNri}$  are the rotation variant and rotation invariant parts of the  $H^{RN}$ .

#### 4. Experimental results

To evaluate the effectiveness of the proposed method, we carried out a series of experiments on two large and comprehensive public texture databases, Outex [32], which includes 24 classes of textures collected under three illuminations and at nine angles, and the Columbia-Utrecht (CURET) database, which contains 61 classes of real-world textures, each imaged under

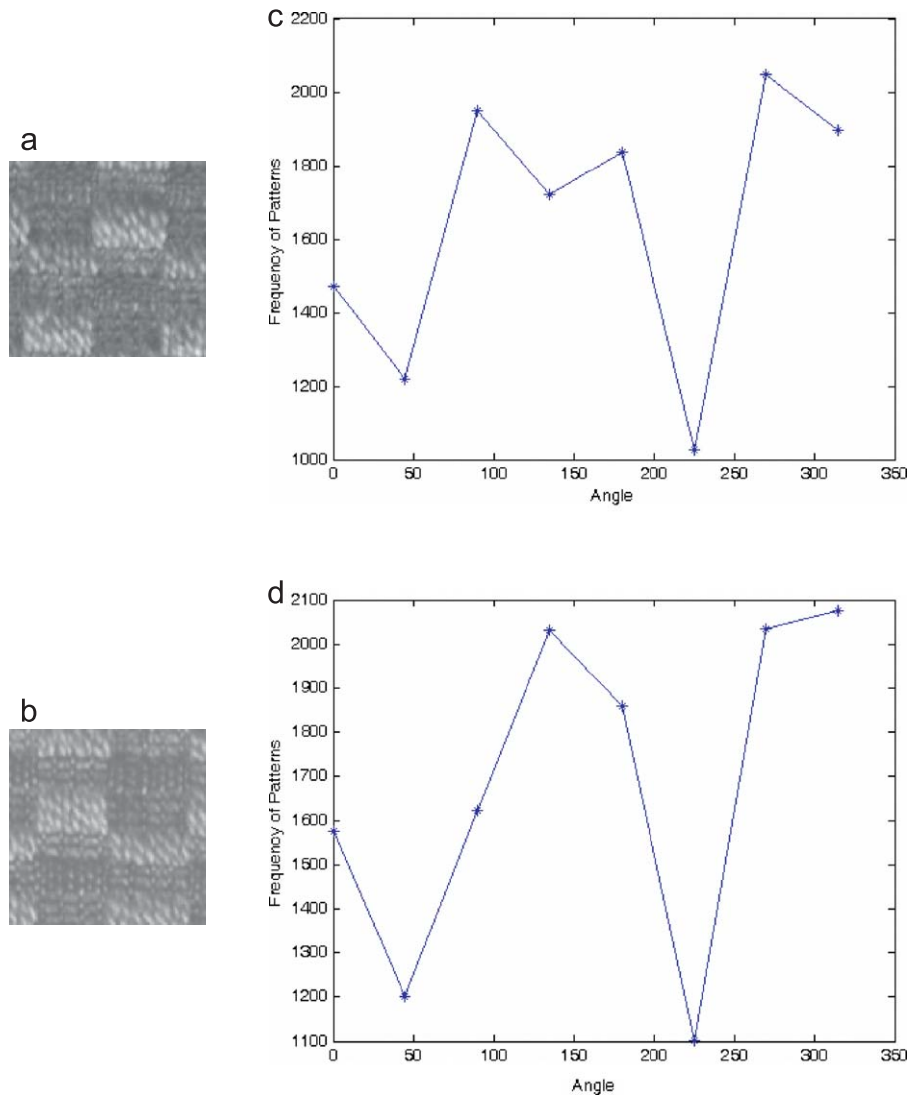


Fig. 7. Two principal orientations texture sample: (a) canvas031 0° [32]; (b) canvas031 0°; (c)  $LBP_{8,1}^{riu2}$  pattern frequency versus angle for image (a); and (d)  $LBP_{8,1}^{riu2}$  pattern frequency versus angle for image (b).

different combinations of illumination and viewing angle [33]. As in [23], we chose 92 sufficiently large images for each class with a viewing angle  $< 60^\circ$ . We used these databases because their texture images were acquired under more varied conditions (viewing angle, orientation and source of illumination) than the widely used Brodatz database.

We evaluated the performance of different methods in terms of classification rate using chi-square distance and the nearest neighborhood classifier. For  $VAR_{P,R}$  and  $LBP_{P,R}^{riu2}/VAR_{P,R}$  quantization we used 128 and 16 bins, respectively, as in [24]. The  $LBP_{P,R}^{riu2}$ ,  $VAR_{P,R}$ ,  $LBP_{P,R}^{riu2}/VAR_{P,R}$  and the state-of-the-art local rotation invariant texture classification algorithm MR8 [23] were used for comparison. In MR8, 10 textons are clustered from each texture class using training samples, and then a histogram based on the  $n \times 10$  textons is computed for each model and sample image, where  $n$  is the number of texture class [23].

In the following, “GM” represents the proposed global matching scheme, while “ES” represents exhaustive search, “PD2” represents using 2 principal orientations for each image and “RN” means preserving RN rows of the rotation variant patterns. If all rows are kept, “RN” will be omitted. For example,  $LBP_{8,1}^{riu2}GM_{ES}$  represents applying exhaustive search to  $LBP_{8,1}^{riu2}$  histogram, while

$LBPV_{8,1}^{iu2}GM_{PD2}^6$  represents using 2 principal orientations and 6 rows of rotation variant patterns of  $LBPV_{8,1}^{iu2}$ . The source codes of the proposed algorithm can be downloaded in [http://www.comp.polyu.edu.hk/~cslzhang/LBPV\\_GM](http://www.comp.polyu.edu.hk/~cslzhang/LBPV_GM).

#### 4.1. Results on the outex database

This section reports the experimental results on two test suites of Outex: Outex\_TC\_00010 (TC10) and Outex\_TC\_00012 (TC12). These two test suites contain the same 24 classes of textures as shown in Fig. 9. Each texture class was collected under three different illuminants (“horizon”, “inca” and “t184”) and nine different angles of rotation ( $0^\circ$ ,  $5^\circ$ ,  $10^\circ$ ,  $15^\circ$ ,  $30^\circ$ ,  $45^\circ$ ,  $60^\circ$ ,  $75^\circ$  and  $90^\circ$ ). There are 20 non-overlapping  $128 \times 128$  texture samples for each class under each setting. Before LBP feature extraction, each  $128 \times 128$  texture sample was normalized to an average intensity of 128 and a standard deviation of 20 [24]. The experimental setups are as follows:

1. For TC10, classifier was trained using samples of illuminant “inca” and  $0^\circ$  angle in each texture class and the classifier was

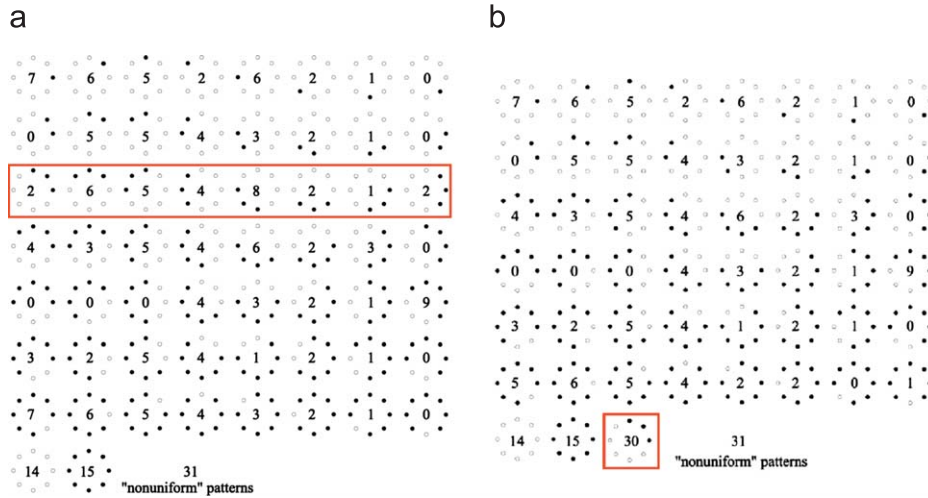


**Fig. 8.** Feature dimensionality reduction. The number in each pattern represents how frequently that pattern occurs in an image: (a) LBP histogram of original image and (b) LBP histogram after feature reduction of (a).

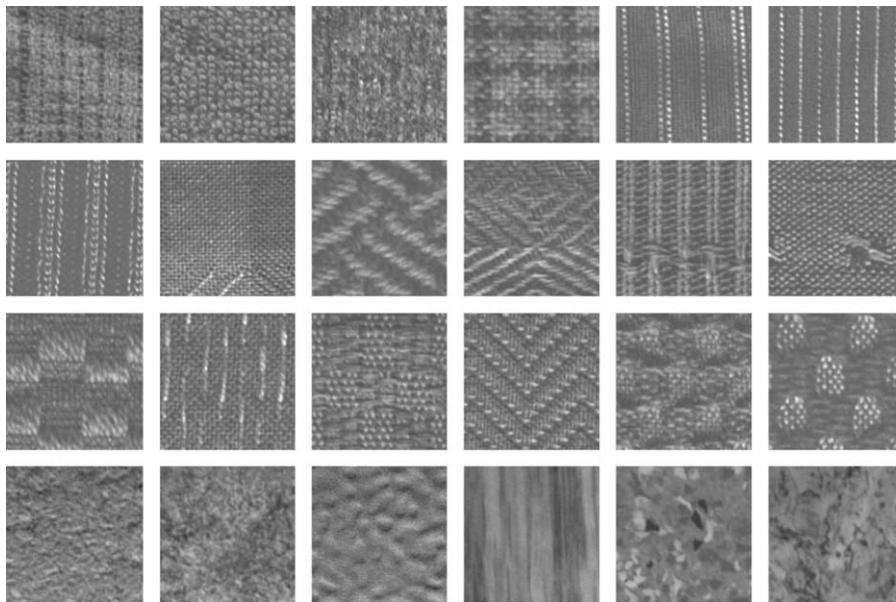


**Fig. 9.** Samples of the 24 textures in TC10 and TC12.

tested using the other eight angles of rotation, under the same illuminant. There are a total of 480 ( $24 \times 20$ ) models and 3,840 ( $24 \times 8 \times 20$ ) validation samples.

- For TC12, the classifier was trained with the same training samples as TC10 and tested with all samples captured under illuminant “t184” or “horizon”. There are a total of 480 ( $24 \times 20$ ) models and 4320 ( $24 \times 20 \times 9$ ) validation samples for each illuminant.

Table 1 presents the results on TC10 and TC12 by different methods. The best results for each test suite are marked in bold font. Based on Table 1, we can make the following four observations.

First, except for  $(P, R)=(8, 1)$ , globally exhaustive search matching has better results than locally rotation invariant feature based matching. The improvement can be very significant. For example,  $LBP_{24,3}^{iu2}GM_{ES}$  achieves 12.7% higher classification rate than  $LBP_{24,3}^{riu2}$  in TC12 (“horizon”). The result for  $(P, R)$  configuration

of  $(8, 1)$  is worse because the angular quantization is  $45^\circ$ , which is coarser than the true rotation angle.

Second, although LBPV has the same feature dimensions as LBP, the use of LBPV adds additional contrast measures to the pattern histogram and this usually produces significantly better results than using LBP. For example, Fig. 10 shows two texture images from different texture classes. Note that they have similar LBP histograms but different LBPV histograms. If  $LBP_{8,1}^{riu2}$  is used, they are put into the same class. However, if  $LBPV_{8,1}^{iu2}$  is used, they are well classified.

Third, the contrast and pattern of a texture are complementary features and so we can expect to get better results using both than using just one alone. As a simplified descriptor of  $LBP_{P,R}^{riu2}/VAR_{P,R}$ ,  $LBPV_{P,R}^{riu2}$  works worse than  $LBP_{P,R}^{riu2}/VAR_{P,R}$  because useful information is lost in the integral projection. However, better results than  $LBP_{P,R}^{riu2}/VAR_{P,R}$  can be obtained by using a suitable matching scheme such as the  $LBPV_{P,R}^{iu2}GM_{ES}$ .

Fourth, the classification performance of locally rotation invariant features,  $LBP_{P,R}^{riu2}$  and  $LBPV_{P,R}^{riu2}$  is 10% worse on average

**Table 1**  
Classification rate (%) for TC10 and TC12 using different methods.

$P, R$	8, 1			16, 2			24, 3		
	TC10	TC12 "t184"	TC12 "horizon"	TC10	TC12 "t184"	TC12 "horizon"	TC10	TC12 "t184"	TC12 "horizon"
$VAR_{P,R}$	90.00	62.93	64.35	86.71	63.47	67.26	81.66	58.98	65.18
$LBP_{P,R}^{riu2} / VAR_{P,R}$	96.66	79.25	77.98	97.83	85.69	84.56	<b>98.15</b>	87.15	87.03
$LBP_{P,R}^{riu2}$	84.89	65.30	63.75	89.24	82.29	75.13	95.18	85.04	80.81
$LBPV_{P,R}^{riu2}$	91.56	76.62	77.01	92.16	87.22	84.86	95.26	91.31	85.04
$LBP_{P,R}^{iu2} GM_{ES}$	66.04	65.37	68.98	89.19	85.94	89.56	97.23	93.49	93.51
$LBPV_{P,R}^{iu2} GM_{ES}$	73.64	72.47	76.57	93.90	90.25	94.28	97.76	<b>95.39</b>	<b>95.57</b>
MR8	92.5 (TC10), 90.9 (TC12, "t184"), 91.1 (TC12, "horizon")								

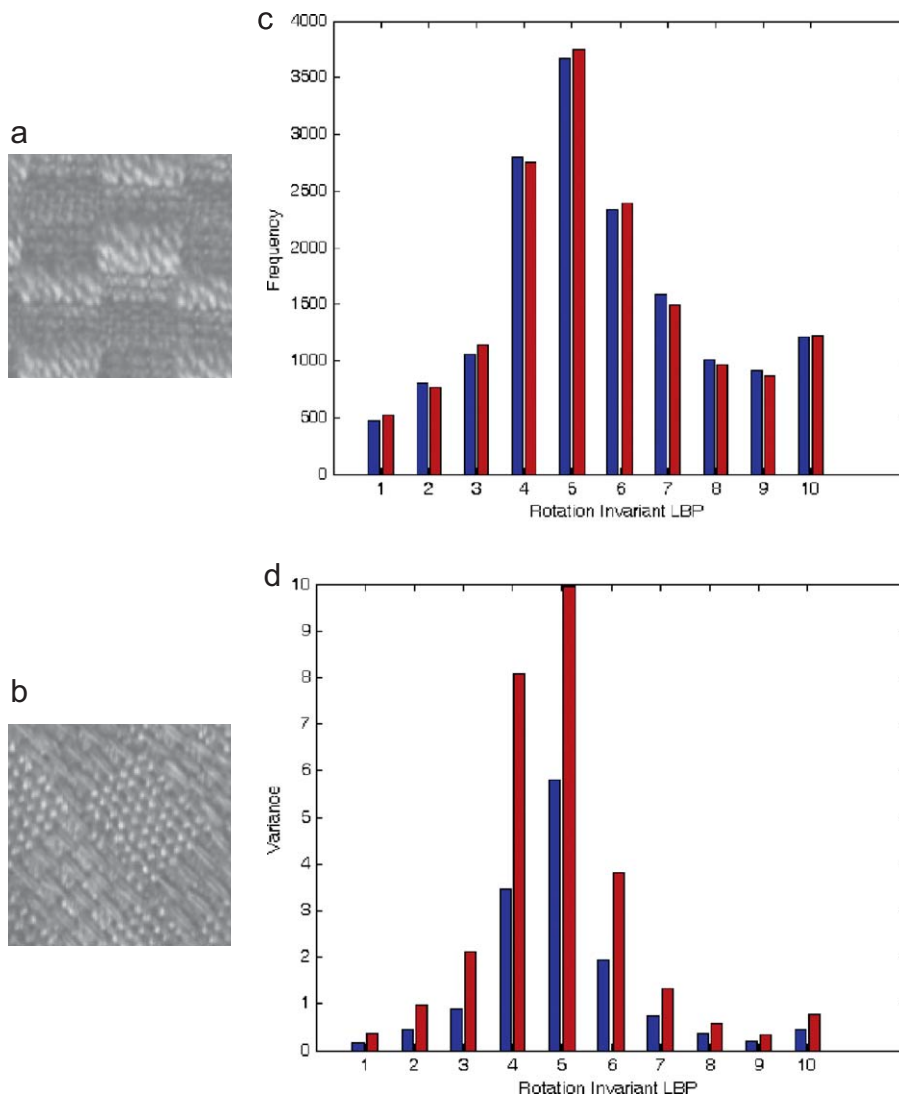


**Fig. 10.** Two texture images with similar LBP histograms but different LBPV histograms.

when the models and samples are captured under different illumination conditions than when they are captured under the same illumination. The performance worsens as the feature size decreases because locally rotation invariant features are very small (for example,  $LBP_{8,1}^{riu2}$  and  $LBPV_{8,1}^{riu2}$  have only 10 bins) and such a small size of features cannot represent each class well. When the difference between textures is very small,  $LBP_{8,1}^{riu2}$  and

$LBPV_{8,1}^{riu2}$  are sensitive to illumination change. This can be seen in the Fisher criterion [35]

$$f = \frac{|\eta_1 - \eta_2|}{\sqrt{\sigma_1^2 + \sigma_2^2}} \quad (18)$$

where  $\eta_1$  and  $\eta_2$  are, respectively, the means of the intra-class and inter-class distances.  $\sigma_1$  and  $\sigma_2$  are, respectively, the standard

deviations of the intra-class and inter-class distances. The Fisher criterion represents the distance between two clusters relative to their size. The larger the Fisher criterion is, the better the separability of the two clusters.

Table 2 lists the Fisher criterion values by different descriptors. The global matching schemes that use rotation variant features, i.e.  $LBP_{P,R}^{u2}GM_{ES}$  and  $LBPV_{P,R}^{u2}GM_{ES}$ , have bigger Fisher criterion values because they have bigger feature sizes and utilize global matching schemes. Since the texture separability are relatively high,  $LBP_{P,R}^{u2}GM_{ES}$  and  $LBPV_{P,R}^{u2}GM_{ES}$  are more robust to illumination change.

Table 3 lists the classification rates by  $LBP_{P,R}^{riu2}/VAR_{P,R}$  on four example classes of textures, two (Canvas026 and Carpet005) having minimal classification rate differences and two (Canvas031 and Canvas038), under different illuminations, having maximal differences. As can be seen in Table 3, Canvas026 and Carpet005 show robustness to illumination variation. The classification rate is perfect even when the illumination changes. However, Canvas031 and Canvas038 are very sensitive to illumination change, and the accuracy drops significantly when the illumination changes. Table 4 lists the average variance measures of these four classes. We see that  $LBP_{P,R}^{riu2}/VAR_{P,R}$  achieves good accuracy on TC10 but bad accuracy on TC12. There are two reasons for this. First, the variations of illumination affect the contrast of textures; second, once the training data has been quantized, it no longer represents the test samples as well. It can be seen that the  $VAR_{P,R}$  change of Canvas026 and Carpet005 is smaller than that of Canvas031 and Canvas038. The large  $VAR_{P,R}$  variation of Canvas031 and Canvas038 makes the quantization

learned from training samples fail to represent the test samples, so the accuracy drops quickly once the illumination changes.

Exhaustive searching is effective but it is time consuming. For example when  $P=24$ , it needs to compute the chi-square distance between two features of  $(24 \times 23 \times 24 + 3) = 13251$  dimensions. One way to speed up matching is to find the principal orientations and match the histogram along the principal orientations only. Table 5 lists the experimental results of using the principal orientations. Since the principal orientations are estimated individually, this process is training-free.

As was demonstrated in the earlier discussion of Fig. 6, the complexity of the structure of image can mean that it is not accurate enough to use just one principal orientation although we can usually accurately represent a texture image using two principal orientations. We see this in Table 5, where keeping two principal orientations achieves very close results to exhaustive search, while the feature dimension of former is only  $\frac{1}{2}$ ,  $\frac{1}{4}$  and  $\frac{1}{6}$  of that of the latter when  $P=8, 16$  and  $24$ , respectively.

To further reduce the feature size, some rotation variant patterns could be clustered into their rotation invariant patterns as discussed in Section 3.3. Fig. 11 shows the classification rates when we use different numbers of rotation variant rows under settings of  $(P, R)=(16, 2)$  and  $(P, R)=(24, 3)$ . When  $RN=0$ , the proposed feature reduction scheme degrades to use local rotation invariant features only, and when  $RN=P-1$ , it does not reduce feature dimension.

We see that the classification rate increases gradually as  $RN$  increases in general. As a tradeoff between accuracy and feature

**Table 2**  
Fisher criterion values by different descriptors.

$P, R$	8, 1			16, 2			24, 3		
	TC10	TC12 "t184"	TC12 "horizon"	TC10	TC12 "t184"	TC12 "horizon"	TC10	TC12 "t184"	TC12 "horizon"
$P, R^{riu2}$	0.77	0.72	0.72	0.90	0.89	0.91	1.03	1.00	1.01
$P, R^{u2}GM_{ES}$	0.82	0.82	0.85	1.14	1.12	1.18	1.29	1.24	1.28
$p, R^{riu2}$	1.02	0.99	1.03	1.06	1.06	1.08	1.09	1.07	1.08
$P, R^{u2}GM_{ES}$	1.06	1.05	1.10	1.26	1.25	1.30	1.34	1.28	1.32

**Table 3**  
 $LBP_{P,R}^{riu2}/VAR_{P,R}$  classification rate (%) under different illuminations and operators.

Class ID	$(P, R)=(8, 1)$			$(P, R)=(16, 2)$			$(P, R)=(24, 3)$		
	TC10	TC12 "t184"	TC12 "horizon"	TC10	TC12 "t184"	TC12 "horizon"	TC10	TC12 "t184"	TC12 "horizon"
Canvas026	100.00	100.00	100.00	100.00	100.00	100.00	100.00	100.00	100.00
Carpet005	100.00	100.00	100.00	100.00	100.00	100.00	100.00	100.00	100.00
Canvas031	98.12	5.00	13.88	99.37	47.22	35.00	100.00	66.11	43.88
Canvas038	100.00	55.00	20.55	100.00	66.66	17.22	100.00	56.11	17.22

**Table 4**  
Average  $VAR_{P,R}$  under different illuminations and operators.

Class ID	$(P, R)=(8, 1)$			$(P, R)=(16, 2)$			$(P, R)=(24, 3)$		
	"inca"	"t184"	"horizon"	"inca"	"t184"	"horizon"	"inca"	"t184"	"horizon"
Canvas026	164.97	163.62	166.64	279.00	275.67	269.79	268.74	266.86	259.24
Carpet005	39.86	38.61	40.74	107.41	104.23	107.77	167.68	163.25	167.15
Canvas031	60.39	65.11	72.15	126.92	135.09	144.35	158.25	165.79	174.00
Canvas038	82.07	91.22	95.35	168.08	184.26	182.91	209.14	225.06	218.21

**Table 5**  
Classification rate (%) using principal orientations.

$P, R$	8, 1			16, 2			24, 3		
	TC10	TC12 "t184"	TC12 "horizon"	TC10	TC12 "t184"	TC12 "horizon"	TC10	TC12 "t184"	TC12 "horizon"
$LBP_{P,R}^{u2} GM_{PD2}^{RN}$	66.04	65.37	68.98	89.19	85.94	89.56	97.23	93.49	93.51
$LBP_{P,R}^{u2} GM_{PD1}$	62.55	63.93	66.85	84.60	80.23	84.28	86.58	78.95	81.11
$LBP_{P,R}^{u2} GM_{PD2}$	66.06	65.25	68.86	89.03	86.01	89.39	96.38	92.03	93.35
$LBPV_{P,R}^{u2} GM_{ES}$	73.64	72.47	76.57	93.90	90.25	94.28	97.76	95.39	95.57
$LBPV_{P,R}^{u2} GM_{PD1}$	65.59	65.30	68.33	89.60	86.29	90.11	95.07	88.72	89.02
$LBPV_{P,R}^{u2} GM_{PD2}$	72.99	72.19	76.15	92.99	89.49	93.95	97.55	94.23	94.18

dimension, in general  $RN=P/2-1$  can be chosen for  $LBP_{P,R}^{u2} GM_{PD2}^{RN}$  and  $LBPV_{P,R}^{u2} GM_{PD2}^{RN}$ . The corresponding feature dimensions are  $(16 \times 7 \times 4 + 3 + 8) = 459$  and  $(24 \times 11 \times 4 + 3 + 12) = 1071$  for  $P=16$  and  $P=24$ , respectively, which are comparable with MR8 ( $(24 \times 10) = 240$ ) and  $LBP_{P,R}^{riu2} / VAR_{P,R}$  ( $((18 \times 16) = 288$  and  $(26 \times 16) = 416$ ). Table 6 lists the classification accuracies when those feature dimensions are used. The accuracies listed in Table 6 are similar to those of  $LBP_{P,R}^{u2} GM_{PD2}$  and  $LBPV_{P,R}^{u2} GM_{PD2}$  listed in Table 1. Interestingly, sometimes, because some trivial features are removed after feature size reduction, the classification rate could be improved a little. For example, with  $(P, R) = (24, 3)$ , the accuracy for TC10 is increased to 98.67% ( $LBP_{P,R}^{u2} GM_{PD2}^{P/2-1}$ ) from 98.15% ( $LBP_{P,R}^{u2} GM_{PD2}$ ).

The proposed feature reduction method needs an unsupervised training procedure to cluster the rows of rotation variant patterns into rotation invariant patterns. Because the most frequent patterns are usually stable across different classes, the proposed feature reduction method is robust to the training set selection. Fig. 12 plots the classification accuracies with  $RN=11$  when  $P=24$ , where the most frequent patterns are determined using different numbers of training classes. Fig. 12 shows that the proposed feature reduction scheme is robust to training sample selection as the variation of classification rate is very small.

#### 4.2. Experimental results on CURET database

The CURET database contains 61 textures, as shown in Fig. 13, and there are 205 images of each texture acquired at different viewpoints and illumination orientations. There are 118 images which have been shot from a viewing angle of  $< 60^\circ$ . Of these 118 images, we selected 92 images, from which a sufficiently large region could be cropped ( $200 \times 200$ ) across all texture classes [23]. We converted all the cropped regions to gray scale and normalized the intensity to zero mean and unit standard deviation to give invariance to global affine transformations in the illumination intensity [23]. Here, instead of computing error bar (i.e. mean and standard deviations of results calculated over multiple splits), the experiments were performed on two different settings to simulate two situations:

1. T46: The 92 images for each class were partitioned evenly into two disjoint training and test sets for a total of 2806 ( $61 \times 46$ ) models and 2806 testing samples.
2. T23: The 92 images for each class were partitioned into two unequal disjoint sets. The training set was formed of the first 23 images for a total of 1403 ( $61 \times 23$ ) models and 4209 ( $61 \times 69$ ) testing samples.

Using the above two settings rather than just one made it possible to better investigate the properties of different operators [23,32]. The T46 setting can simulate the situation when we have comprehensive training samples while the T23 setting can

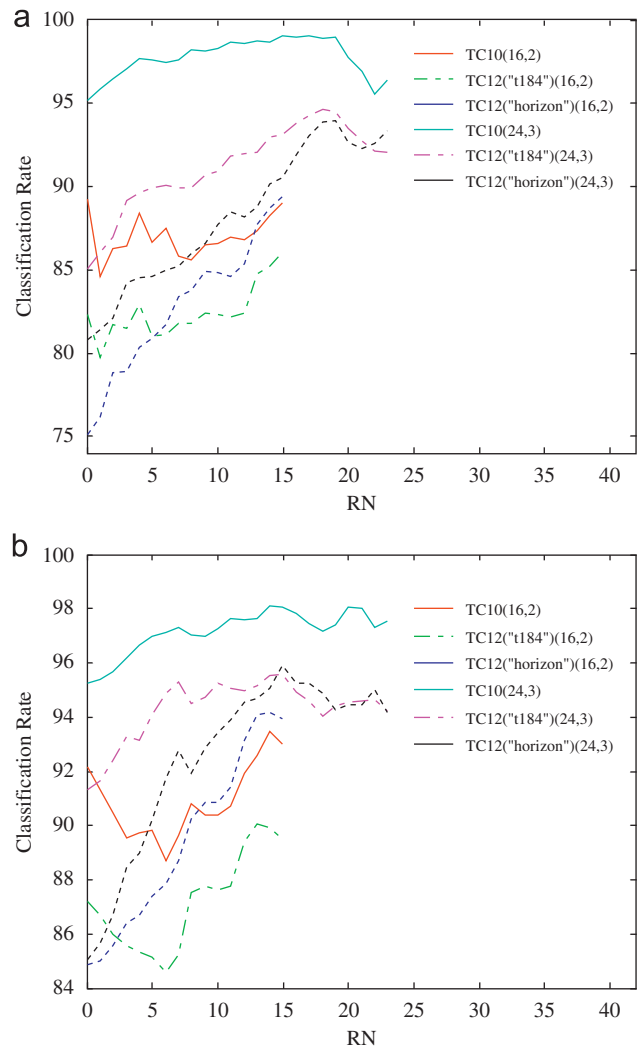


**Fig. 11.** Classification rates when using different numbers of rows. (a)  $LBP_{P,R}^{u2} GM_{PD2}^{RN}$  with different number of RN and (b)  $LBPV_{P,R}^{u2} GM_{PD2}^{RN}$  with different number of RN.

simulate the situation when we have only partial training samples. Table 7 lists the classification results by different operators. The best accuracy for different settings is marked in bold.

Table 7 presents similar findings to those in Table 1, such as LBPV being better than LBP, global matching schemes improving accuracy,  $LBP_{P,R}^{riu2} / VAR_{P,R}$  being sensitive to training sample selection, etc. In this database MR8 gets the best result in the T46 test suite. This is because MR8 is a statistical approach and fortunately comprehensive training samples are available in this database to

**Table 6**  
Classification rate (%) when  $RN=P/2-1$ .

$P, R$	8, 1			16, 2			24, 3		
	TC10	TC12 "t184"	TC12 "horizon"	TC10	TC12 "t184"	TC12 "horizon"	TC10	TC12 "t184"	TC12 "horizon"
$LBP_{P,R}^{riu2} GM_{PD2}^{P/2-1}$	76.43	67.80	69.67	85.80	81.75	83.42	98.67	91.85	88.49
$LBPV_{P,R}^{riu2} GM_{PD2}^{P/2-1}$	89.32	80.94	78.84	89.63	85.23	88.68	97.63	95.06	93.88

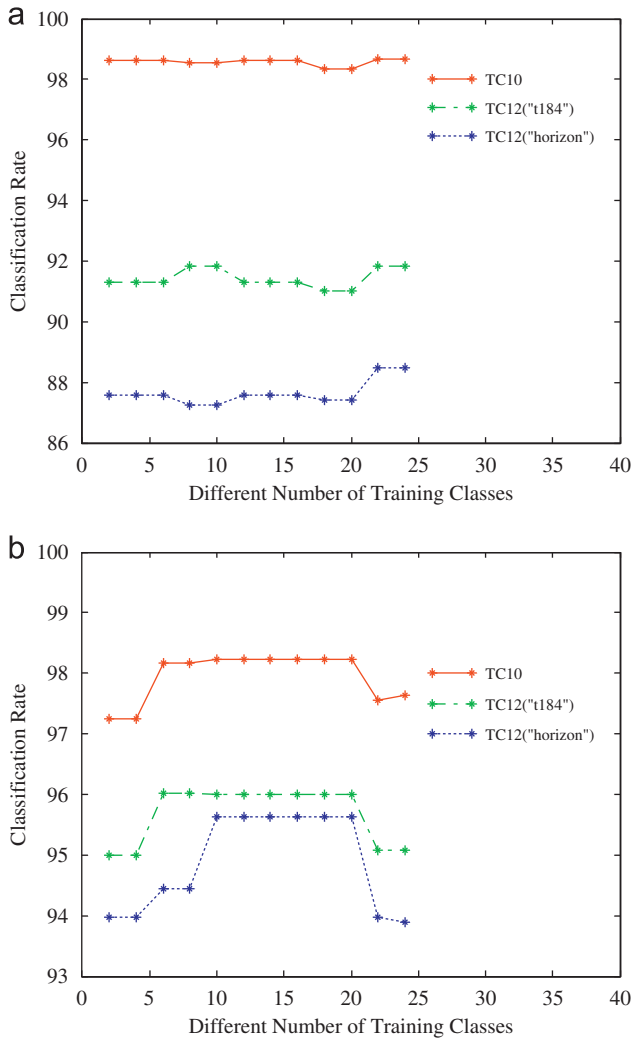


**Fig. 12.** The classification accuracy of feature reduction under different training setting. (a)  $LBP_{24,3}^{riu2} GM_{PD2}^{11}$  accuracy vs. the training class number and (b)  $LBPV_{24,3}^{riu2} GM_{PD2}^{11}$  accuracy vs. the training class number.

find representative textons. However, if this condition could not be satisfied, its accuracy would decrease, such as in T23 and in Outex (see Section 4.1).

Multiresolution analysis could be used to improve the classification accuracy, that is, by employing multiple operators of varying  $(P, R)$ . In this study, we use a straightforward multiresolution analysis that measures the dissimilarity as the sum of chi-square distances from all operators [24]:

$$D_N = \sum_{n=1}^N D(S^n, M^n) \quad (19)$$

where  $N$  is the number of operators, and  $S^n$  and  $M^n$  are, respectively, the sample and model histograms extracted with the  $n$ th ( $n = 1, \dots, N$ ) operator.

As can be seen in Table 8, multiresolution analysis is a simple but effective way to increase the accuracy of LBP and LBPV. The classification rates can be improved to 96.04% for T46 and 81.77% for T23. Of the different multiresolution operators, “(8, 1)+(24, 3)” gets the best results in most cases. This is because there are redundancies between LBP patterns of different radius, while (8, 1) and (24, 3) have fewer redundancies. This also explains why using three operators may not get better results than using two.

### 4.3. Comparison of LBP based methods and MR8 method

Both LBP-based and MR8 methods classify an image in three steps: feature extraction, histogram creation, and classification. In the feature extraction stage, while LBP uses a nonlinear filter or a series of linear filters [29] to form the pattern, and uses a nonlinear filter to measure the contrast for each pixel, MR8 requires 38 linear filters to extract an 8-dimensional feature vector for each pixel.

It is simple and fast to build a traditional LBP histogram. It is not so simple for MR8, which must find for each pixel the most similar texton from a learned dictionary (240 textons for Outex and 610 textons for CURET). Its histogram is built based on the texton frequency. This process is time consuming, especially when the feature vector is long and the size of texton dictionary is large.

MR8 and LBP based methods using the same dissimilarity measure and classifier. The only difference is the dimensions of the histogram. The main drawback of the proposed matching schemes is relatively big feature size. When the number of models increases, comparison takes longer time. However, the proposed feature dimension reduction method can significantly reduce the feature size. For example, the feature size of  $LBP_{24,3}^{riu2} GM_{PD2}^{11}$  is 1071, only several times the feature sizes of  $LBP_{24,3}^{riu2} / VAR_{24,3}$  (416) and MR8 (240 for Outex and 610 for CURET). In addition, there are methods to reduce the number of models of each texture class, such as the SOM algorithm [34] and the greedy algorithm [23]. Usually, it is possible to get better accuracy by removing some outlier models [23,34].

## 5. Conclusion

To better exploit the local and global information in texture images, this paper proposed a novel hybrid LBP scheme, globally rotation invariant matching with locally variant LBP features, for texture classification. Based on LBP distribution, the principal orientations of the texture image were first estimated, and then the LBP histograms can be aligned. These histograms were in turn used to measure the dissimilarity between images. A new texture descriptor, namely LBP variance (LBPV) was proposed to improve the performance of LBP by exploiting the local contrast information. Finally, a feature size reduction method was proposed to speed up the matching scheme.

The experimental results on two large databases demonstrated that the proposed global rotation invariant matching scheme with rotation variant LBP or LBPV feature leads to much higher classification accuracy than traditional rotation invariant LBP.

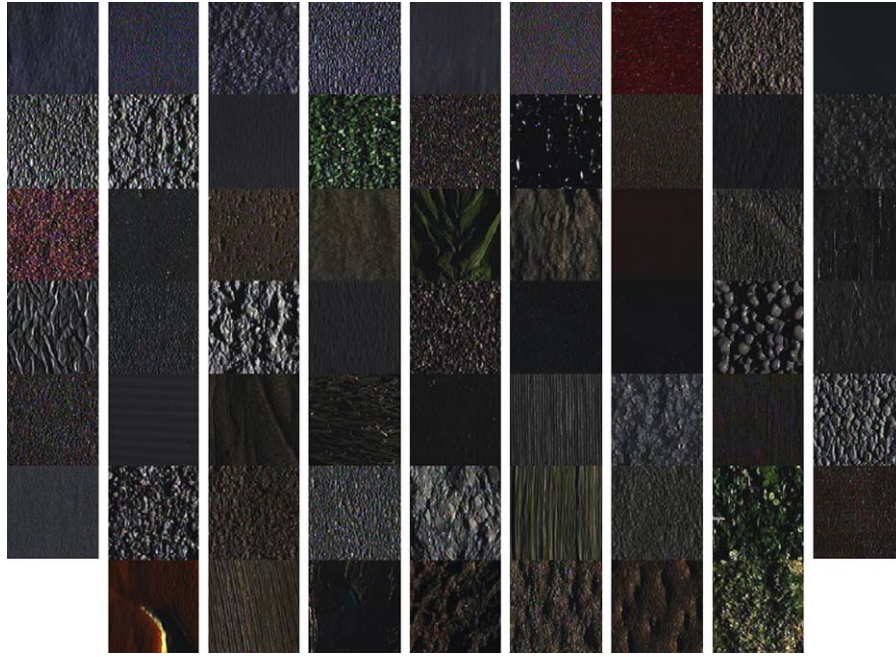


**Fig. 13.** Textures from the Columbia–Utrecht database. In this work, all images are converted to monochrome so color is not used to discriminate between different textures.

**Table 7**  
Classification rates (%) using different operators.

$P, R$	8, 1		16, 2		24, 3	
	T46	T23	T46	T23	T46	T23
$VAR_{P,R}$	69.17	44.73	64.61	41.29	63.22	39.15
$LBP_{P,R}^{riu2} / VAR_{P,R}$	93.65	70.70	93.90	70.82	93.90	70.91
$LBP_{P,R}^{riu2}$	81.61	57.97	85.56	63.55	87.38	66.59
$LBPV_{P,R}^{riu2}$	88.23	71.56	89.77	73.10	91.09	74.26
$LBP_{P,R}^{iu2} GM_{PD2}^{p/2-1}$	89.41	66.90	93.44	74.86	90.80	71.77
$LBPV_{P,R}^{iu2} GM_{PD2}^{p/2-1}$	93.19	75.26	94.15	<b>79.66</b>	92.97	76.69
MR8	<b>97.54</b> (T46), 77.57 (T23)					

**Table 8**  
Classification rates (%) of multiresolution analysis.

$P, R$	(8, 1)+(16, 2)		(8, 1)+(24, 3)		(16, 2)+(24, 3)		(8, 1)+(16, 2)+(24, 3)	
	T46	T23	T46	T23	T46	T23	T46	T23
$LBP_{P,R}^{riu2}$	91.55	70.82	94.04	74.22	91.30	71.01	93.83	74.36
$LBP_{P,R}^{iu2} GM_{PD2}^{p/2-1}$	95.11	76.00	95.36	77.80	93.97	76.76	95.58	78.21
$VAR_{P,R}$	71.31	47.96	73.55	50.22	63.36	42.50	67.46	47.37
$LBP_{P,R}^{riu2} / VAR_{P,R}$	95.18	72.74	<b>96.04</b>	74.50	94.51	72.29	95.61	74.38
$LBPV_{P,R}^{riu2}$	93.47	78.28	94.65	80.16	92.76	76.45	94.47	79.94
$LBPV_{P,R}^{iu2} GM_{PD2}^{p/2-1}$	95.36	<b>81.77</b>	<b>96.04</b>	81.37	95.26	80.01	<b>96.04</b>	81.58

Meanwhile, using two principal orientations for matching could achieve similar result to that by exhaustive searching and this reduces much the searching space. As a simplified version of LBP/VAR, the proposed LBPV achieves much better results than LBP and higher accuracy than LBP/VAR in coupling with the global matching scheme. The proposed feature dimension reduction scheme based

on distance measurement could reduce the feature size significantly while keeping the classification performance good enough.

## Acknowledgments

The authors sincerely thank MVG and VGG for sharing the source codes of LBP and MR8. The work is partially supported by the GRF fund from the HKSAR Government, the central fund from Hong Kong Polytechnic University, the Natural Scientific Research Innovation Foundation in Harbin Institute of Technology, Key Laboratory of Network Oriented Intelligent Computation (Shenzhen), the NSFC (nos. 60620160097, 60803090), the 863 (no. 2006AA01Z193), and SZHK-innovation funds (SG200810100003A). We would like to thank the anonymous reviewers for their constructive comments.

## References

- [1] M. Tuceryan, A.K. Jain, Texture Analysis, in: C.H. Chen, L.F. Pau, P.S.P. Wang (Eds.), Handbook of Pattern Recognition and Computer Vision, World Scientific Publishing Co., Singapore, 1993, pp. 235–276 (Chapter 2).
- [2] F.S. Cohen, Z. Fan, S. Attali, Automated inspection of textile fabrics using textural models, IEEE Transactions on Pattern Analysis and Machine Intelligence 13 (8) (1991) 803–808.
- [3] H. Anys, D.C. He, Evaluation of textural and multipolarization radar features for crop classification, IEEE Transactions on Geoscience and Remote Sensing 33 (5) (1995) 1170–1181.
- [4] Q. Ji, J. Engel, E. Craine, Texture analysis for classification of cervix lesions, IEEE Transactions on Medical Imaging 19 (11) (2000) 1144–1149.
- [5] R.M. Haralik, K. Shanmugam, I. Dinstein, Texture features for image classification, IEEE Transactions on Systems, Man, and Cybernetics 3 (6) (1973) 610–621.
- [6] T. Randen, J.H. Husy, Filtering for texture classification: a comparative study, IEEE Transactions on Pattern Analysis and Machine Intelligence 21 (4) (1999) 291–310.
- [7] A.C. Bovik, M. Clark, W.S. Geisler, Multichannel texture analysis using localized spatial filters, IEEE Transactions on Pattern Analysis and Machine Intelligence 12 (1) (1990) 55–73.
- [8] B.S. Manjunath, W.Y. Ma, Texture features for browsing and retrieval of image data, IEEE Transactions on Pattern Analysis and Machine Intelligence 18 (8) (1996) 837–842.

- [9] T. Chang, C.C.J. Kuo, Texture analysis and classification with tree-structured wavelet transform, *IEEE Transactions on Image Processing* 2 (4) (1993) 429–441.
- [10] A. Laine, J. Fan, Texture classification by wavelet packet signatures, *IEEE Transactions on Pattern Analysis and Machine Intelligence* 15 (11) (1993) 1186–1191.
- [11] M. Unser, Texture classification and segmentation using wavelet frames, *IEEE Transactions on Image Processing* 4 (11) (1995) 1549–1560.
- [12] R.L. Kashyap, A. Khotanized, A model-based method for rotation invariant texture classification, *IEEE Transactions on Pattern Analysis and Machine Intelligence* 8 (4) (1986) 472–481.
- [13] J. Mao, A.K. Jain, Texture classification and segmentation using multi-resolution simultaneous autoregressive models, *Pattern Recognition* 25 (2) (1992) 173–188.
- [14] J.L. Chen, A. Kundu, Rotation and gray scale transform invariant texture identification using wavelet decomposition and hidden Markov model, *IEEE Transactions on Pattern Analysis and Machine Intelligence* 16 (2) (1994) 208–214.
- [15] W.R. Wu, S.C. Wei, Rotation and gray-scale transform-invariant texture classification using spiral resampling, subband decomposition, and hidden Markov model, *IEEE Transactions on Image Processing* 5 (10) (1996) 1423–1434.
- [16] R. Porter, N. Canagarajah, Robust rotation-invariant texture classification: wavelet, Gabor, and GMRF based schemes, *IEE Proceedings Vision, Image, and Signal Processing* 144 (3) (1997) 180–188.
- [17] H. Arof, F. Deravi, Circular neighbourhood and 1-D DFT features for texture classification and segmentation, *IEE Proceedings Vision, Image, and Signal Processing* 145 (3) (1998) 167–172.
- [18] T.N. Tan, Rotation invariant texture features and their use in automatic script identification, *IEEE Transactions on Pattern Analysis and Machine Intelligence* 20 (7) (1998) 751–756.
- [19] G.M. Hayley, B.M. Manjunath, Rotation invariant texture classification using a complete space–frequency model, *IEEE Transactions on Image Processing* 8 (2) (1999) 255–269.
- [20] P. Campisi, A. Neri, C. Panci, G. Scarano, Robust rotation-invariant texture classification using a model based approach, *IEEE Transactions on Image Processing* 13 (6) (2004) 782–791.
- [21] H. Deng, D.A. Clausi, Gaussian MRF rotation-invariant features for image classification, *IEEE Transactions on Pattern Analysis and Machine Intelligence* 26 (7) (2004) 951–955.
- [22] K. Jafari-Khouzani, H. Soltanian-Zadeh, Radon transform orientation estimation for rotation invariant texture analysis, *IEEE Transactions on Pattern Analysis and Machine Intelligence* 27 (6) (2005) 1004–1008.
- [23] M. Varma, A. Zisserman, A statistical approach to texture classification from single images, *International Journal of Computer Vision* 62 (1–2) (2005) 61–81.
- [24] T. Ojala, M. Pietikäinen, T.T. Mäenpää, Multiresolution gray-scale and rotation invariant texture classification with local binary pattern, *IEEE Transactions on Pattern Analysis and Machine Intelligence* 24 (7) (2002) 971–987.
- [25] N. Kim, S. Udpa, Texture classification using rotated wavelet filters, *IEEE Transactions on Systems, Man and Cybernetics, Part A: Systems and Humans* 30 (6) (2000) 847–852.
- [26] M. Kokare, P.K. Biswas, B.N. Chatterji, Rotation-invariant texture image retrieval using rotated complex wavelet filters, *IEEE Transactions on Systems, Man and Cybernetics, Part B: Cybernetics* 36 (6) (2006) 1273–1282.
- [27] V. Kyrki, J.K. Kamarainen, Simple Gabor feature space for invariant object recognition, *Pattern Recognition Letter* 25 (3) (2004) 311–318.
- [28] N.G. Kingsbury, Rotation-invariant local feature matching with complex wavelets, in: 14th European Signal Processing Conference, 2006.
- [29] T. Ahonen, M. Pietikäinen, A framework for analyzing texture descriptors, in: *International Conference on Computer Vision Theory and Applications*, 2008, pp. 507–512.
- [30] R. Brunelli, T. Poggio, Face recognition: features versus templates, *IEEE Transactions on Pattern Analysis and Machine Intelligence* 15 (10) (1993) 1042–1052.
- [31] M. Varma, A. Zisserman, Unifying statistical texture classification framework, *Image and Vision Computing* 22 (14) (2004) 1175–1183.
- [32] T. Ojala, T. Mäenpää, M. Pietikäinen, J. Viertola, J. Kyllönen, S. Huovinen, Outex—new framework for empirical evaluation of texture analysis algorithm, in: *International Conference on Pattern Recognition*, 2002, pp. 701–706.
- [33] K.J. Dana, B. van Ginneken, S.K. Nayar, J.J. Koenderink, Reflectance and texture of real world surfaces, *ACM Transactions on Graphics* 18 (1) (1999) 1–34.
- [34] M. Pietikäinen, T. Nurmela, T. Mäenpää, M. Turtinen, View-based recognition of real-world textures, *Pattern Recognition* 37 (2) (2004) 313–323.
- [35] K. Fukunaga, *Introduction to Statistical Pattern Recognition*, Academic, New York, 1990.
- [36] S. Lazebnik, C. Schmid, J. Ponce, A sparse texture representation using local affine regions, *IEEE Transactions on Pattern Analysis and Machine Intelligence* 27 (8) (2005) 1265–1278.
- [37] Y. Xu, H. Ji, C. Fermuller, A projective invariant for texture, in: *International Conference on Computer Vision and Pattern Recognition*, 2006, pp. 1932–1939.
- [38] M. Mellor, B. Hong, M. Brady, Locally rotation, contrast, and scale invariant descriptors for texture analysis, *IEEE Transactions on Pattern Analysis and Machine Intelligence* 30 (1) (2008) 52–61.

**About the Author**—ZHENHUA GUO received the B.S. and M.S. degree in Computer Science from Harbin Institute of Technology in 2002 and 2004, respectively. From 2005 to 2007, he was a Research Assistant with the Department of Computing, the Hong Kong Polytechnic University. Since August 2007, he has been a Ph.D. candidate at Department of Computing, the Hong Kong Polytechnic University. His research interests include pattern recognition, texture classification, biometrics, etc.

**About the Author**—LEI ZHANG received the B.S. degree in 1995 from Shenyang Institute of Aeronautical Engineering, Shenyang, PR China, the M.S. and Ph.D. degrees in Control Theory and Applications from Northwestern Polytechnical University, Xi'an, PR China, respectively, in 1998 and 2001. From 2001 to 2002, he was a Research Associate in the Department of Computing, The Hong Kong Polytechnic University. From January 2003 to January 2006 he worked as a Postdoctoral Fellow in the Department of Electrical and Computer Engineering, McMaster University, Canada. Since January 2006, he has been an Assistant Professor in the Department of Computing, The Hong Kong Polytechnic University. His research interests include image and video processing, biometrics, pattern recognition, multisensor data fusion and optimal estimation theory, etc.

**About the Author**—DAVID ZHANG graduated in Computer Science from Peking University in 1974 and received his M.Sc. and Ph.D. degrees in Computer Science and Engineering from the Harbin Institute of Technology (HIT), Harbin, PR China, in 1983 and 1985, respectively. He received the second Ph.D. degree in Electrical and Computer Engineering at the University of Waterloo, Waterloo, Canada, in 1994. From 1986 to 1988, he was a Postdoctoral Fellow at Tsinghua University, Beijing, China, and became an Associate Professor at Academia Sinica, Beijing, China. Currently, he is a Chair Professor with the Hong Kong Polytechnic University, Hong Kong. He was elected as an IEEE Fellow on 2009. He is the Founder and Director of Biometrics Research Center supported by the Government of the Hong Kong SAR (UGC/CRC). He is also the Founder and Editor-in-Chief of the *International Journal of Image and Graphics (IJIG)*, Book Editor, *The Kluwer International Series on Biometrics*, and the Associate Editor of several international journals. His research interests include automated biometrics-based authentication, pattern recognition, biometric technology and systems. As a principal investigator, he has finished many biometrics projects since 1980. So far, he has published over 200 papers and 10 books.